J. Fluid Mech. (1972), *vol.* 53, *part* 1, *pp.* 85–111
Printed in Great Britain

The internal structure of shock waves

By BRUCE L. HICKS, SHEE-MANG YEN AND BARBARA J. REILLY
Co-ordinated Science Laboratory, University of Illinois

(Received 13 April 1971)

The nonlinear Boltzmann equation has been solved for shock waves in a gas of elastic spheres. The solutions were made possible by the use of Nordsieck's Monte Carlo method of evaluation of the collision integral in the equation. Accurate solutions were obtained by the same numerical procedure for eight values of the upstream Mach numbers M_1 ranging from 1·1 to 10, even though the corresponding degree of departure from equilibrium varies by a factor greater than 100. Many more characteristics of the internal structure of the shock waves have been calculated from the solutions than have hitherto been available. Each solution of the Boltzmann equation requires about 10^8 multiplications to obtain statistical errors of 3 % in values of the velocity distribution function and collision integral and much smaller errors in the moments of these functions.

The reciprocal shock thickness is in agreement with that of the Mott-Smith shock (u^2 moment) from $M_1 = 2{\cdot}5$–8. The density profile is asymmetric with an upstream relaxation rate (measured as density change per mean free path) approximately twice as large as the downstream value for weak shocks and equal to the downstream value for strong shocks. The temperature density relation is in agreement with that of the Navier–Stokes shocks for Mach numbers in the range 1·1–1·56. The Boltzmann reciprocal shock thickness is smaller than the Navier–Stokes value in this range of Mach number because the viscosity–temperature relation computed is not constant as predicted by the linearized theory.

The velocity moments of the distribution function are, like the Mott-Smith shock, approximately linear with respect to the number density; however, the deviations from linearity are statistically significant. Four functionals of the distribution function that are discussed show maxima within the shock. The entropy is a good approximation to the Boltzmann function for all M_1. The solutions obtained satisfy the Boltzmann theorem for all Mach numbers. The ratio of total heat flux q to q_x (that associated with the longitudinal degree of freedom) correlates well with local Mach number for all M_1 in accordance with a relation derived by Baganoff & Nathenson (1970). The Chapman–Enskog linearized theory predicts that this ratio is constant. The (effective) transport coefficients are larger than the Chapman–Enskog equivalents by as much as a factor of three at the mid-shock position.

At $M_1 = 4$, and for 40 % of the velocity bins, the distribution function is different from the corresponding Mott-Smith value by more than three times the 90 % confidence limit. The r.m.s. value of the percentage difference in distribution

functions is 15 % for this Mach number. At $M_1 = 1{\cdot}59$, the half width and several other characteristics of the function

$$\int f\,dv_y\,dv_z$$

differ from that of the Chapman–Enskog first iterate, and many of the deviations are in agreement with an experiment by Muntz & Harnett (1970).

1. Introduction

A shock wave is a commonly occurring, well-defined, non-equilibrium phenomenon in gasdynamics. It is therefore desirable to be able to determine any of its properties that are currently of physical interest and to be able to determine others as they are needed in the future. Unfortunately, experiment yields only a few properties of shock waves and, until recently, calculations of the structure of strong shocks have been based upon assumptions whose validity has not been established.

Nordsieck's development, more than a decade ago, of an *accurate* Monte Carlo method of evaluation of the collision integral in the nonlinear Boltzmann equation radically altered this situation, both for shock wave calculations and for other problems in rarefied gasdynamics. No longer is it necessary to assume near-equilibrium or nearly free-molecule flow, nor to assume the validity of equations substituted for the full nonlinear Boltzmann equation. Nordsieck's evaluation of the collision term (gain and loss terms separately) makes possible direct solution† of this basic equation, a possibility that has been largely ignored in the century since the equation was derived by Boltzmann.

Nordsieck's method was developed in 1958 and was first described in the literature in 1967 (Nordsieck & Hicks 1967). Brief accounts of the application of the method to strong shock waves have appeared there and in the *Proceedings of the Sixth Rarefied Gas Dynamics Symposium* (Hicks & Yen 1969). Applications to other problems have also been made (Hicks 1965; Yen & Hicks 1967*a*, *b*; Yen 1971; Yen & Schmidt 1969). Part of an extensive analysis of the systematic and random errors of the method and its applications was published in Hicks & Smith (1968). More recent analyses of the errors and improvements of the method have been described in a report (Hicks, Yen & Reilly 1969).

Using Monte Carlo evaluation of the nonlinear collision integrals, during the period 1967–70 we solved the nonlinear Boltzmann equation for shock waves in a gas of elastic spheres. We used the same numerical methods for eight Mach

† By solution of the Boltzmann equation we mean calculation and line-printer output of (i) accurate numerical values of the velocity distribution function $f(\mathbf{v}, x)$ for each of 226 cells in velocity space and for each of 9–17 positions in the shock wave, and (ii) estimates of the probable (statistical) error of *each* of these values of $f(\mathbf{v}, x)$, of each of the corresponding values of the gain and loss terms in the collision integral $a - bf$ and of *each* of some 100 functions derived from f, a and bf. These functions include all the functions that are often regarded as 'solutions' of the Boltzmann equation. By the adjective accurate we imply that the probable errors in $f(\mathbf{v}, x)$ are about 3 % on the average. These matters have been discussed in some detail in Hicks & Smith (1967, 1968) and Hicks *et al.* (1969).

numbers in the range 1·1–10. In the present paper we describe selected results from these calculations.

There are several reasons for publishing only selected results of these shock wave calculations, the most obvious being the large volume of results, larger than it is possible to print in a journal. Furthermore, no definitive comparisons with experimental results are possible until a new theory that predicts the effects upon the collision integral of changing the intermolecular forces is developed or until differential cross-sections for realistic, slightly 'soft' molecular fields are known. It is also impossible to predict exactly which detailed computed properties of shock structure will be needed in the future to compare with other calculations and with experiment. However, using our basic Boltzmann program, which solves the Boltzmann equation accurately, and the AVERR program, which gives detailed information about moments and functions derived from them, we can relatively easily calculate the specific details of shock structure *when they are needed.*

For these reasons we have chosen to describe here those characteristics of shock waves having the greatest physical interest at present. These characteristics are named in the section headings. With one exception (§ 2) we discuss first those characteristics which are most commonly treated in gasdynamics, namely, shock thickness and density gradients. We then discuss progressively less familiar characteristics: thermodynamic properties, gradients of temperature and of the Boltzmann flux, transport properties (including two components of heat flux), the distribution function and the collision integral itself.

It is useful to preface our discussion of these characteristics with general remarks on our methods. For a number of reasons (see Hicks & Smith 1967) we find it desirable to use the *local particle density* n as the independent variable rather than x, the position co-ordinate. Except in § 3, then, we consider variations of the different shock properties as functions of n rather than of x. We often use dimensionless variables like $\hat{n} = (n-n_1)/(n_2-n_1)$.

The solutions we discuss are iterative solutions of the Boltzmann *difference* equation, which we have reason to believe approximate well the solutions of the *differential* equation (Hicks & Smith 1967, 1968). The difference equation is solved by embedding Nordsieck's Monte Carlo method of evaluating the collision integral in an iterative scheme for finding velocity distribution functions (everywhere in the shock wave and at all positions in velocity space) which produces two sides of the Boltzmann equation that are equal within about 1%. We have studied the convergence of the iterative scheme and made strong uniqueness tests of our solutions. The results of weaker tests have already been published (Hicks & Smith 1968).

The units used are the values, denoted by the subscript 1, of various properties of the upstream gas. Thus n_1 and t_1 are the units of number density n and temperature t, the unit of length $l_1 = 1/(2\pi n_1 \sigma^2) = (\text{mean free path})_1/\sqrt{2}$ and the unit velocity $c_1 = (2\pi k t_1/m)^{\frac{1}{2}} = (\text{mean speed})_1 \times \frac{1}{2}\pi$. The unit of time is therefore $(\text{mean free time})_1 \times (2/\pi)^{\frac{1}{2}}$ and the unit of the velocity distribution function is n_1/c_1^3. In these units the Boltzmann equation for the shock wave is

$$v_x \partial f/\partial x = a - bf = \int (FF' - ff')\,|\mathbf{k}.\mathbf{v}_r|\,d\mathbf{v}'(d\mathbf{k}/4\pi),$$

where $f = f(\mathbf{v}, x)$ is the velocity distribution function, x is the distance in the direction perpendicular to the shock, the unit vector $\mathbf{k}$ gives the direction of the line of centres during a collision, $\mathbf{v}_r = \mathbf{v}' - \mathbf{v}$ and f, f', F and F' denote the four values of f corresponding to the four velocities $\mathbf{v}$, $\mathbf{v}'$, $\mathbf{V}$ and $\mathbf{V}'$. Integration is over the whole 4π solid angle in order that the $\mathbf{k}$ integration limits may be independent of $\mathbf{v}$ and $\mathbf{v}'$. The term bf reminds us that this second part of the collision integral is proportional to $f(\mathbf{v}, x)$, a fact of importance in devising a stable method of integrating the differential equation.

In all calculations we used 226 bins in the $(v_x, v_\perp)$ velocity space, where v_x and $v_\perp$ are components in cylindrical co-ordinates. For this subdivision of velocity space it is possible to make meaningful calculations up to a Mach number $M_1 = 10$ but not much higher. We used the LS and the MB corrections and the 'single sample' technique (Hicks *et al.* 1969) throughout the calculations in the entire M_1 range of 1·1–10. For each M_1, runs were made for each of four large independent collision samples (2^{13} collisions per sample), yielding estimates of the mean value and the statistical error of *any* quantity derived from either the velocity distribution functions or the collision integrals. The r.m.s. probable errors of the (mean) velocity distribution function, calculated by our solution of the Boltzmann equation, were determined for each Mach number and are about 3 % for a Mach number of 4. The probable errors in various (mean) moments of the velocity distribution and of the collision integral are smaller by factors of ten to one hundred. This level of accuracy is obtained on the CDC 1604 digital computer (50 μs multiplication time) in a run lasting about 2 h for each Mach number (equivalent to $1{\cdot}4 \times 10^8$ multiplications). Calculations of each value of a or bf, that is, each value of a fivefold integral, requires only the time for about 2000 multiplications per iteration.

The values of the mean and the statistical error of each function derived from the velocity distribution function or the collision integral is calculated by the AVERR program. This program computes the means and errors of 100 functions for each set of four collision samples, for each position in the shock and for each value of the Mach number. We discuss seventeen of these functions in later sections of the paper.

The overall method is summarized in figure 1. As shown in this figure, thermodynamic properties and transport properties of shock waves are calculated from the moments of the distribution function, gradients from the moments of the collision integrals, and transport coefficients from both types of moments. One moment of f, namely n, the number density, is taken to be the independent variable in most sections of the paper.

We have tested the accuracy of the Mott-Smith solutions in satisfying the Boltzmann equation and have found that our Monte Carlo solutions satisfy the Boltzmann equation more accurately by a factor of 100. Since we know the magnitudes of the random errors of our solutions we can state unequivocally, in the comparison with the Mott-Smith solution, which differences may be significant and which are not. The comparison with the Mott-Smith results is of interest because we have found that the qualitative features of the Mott-Smith velocity distribution functions are correct and that some of the Mott-Smith

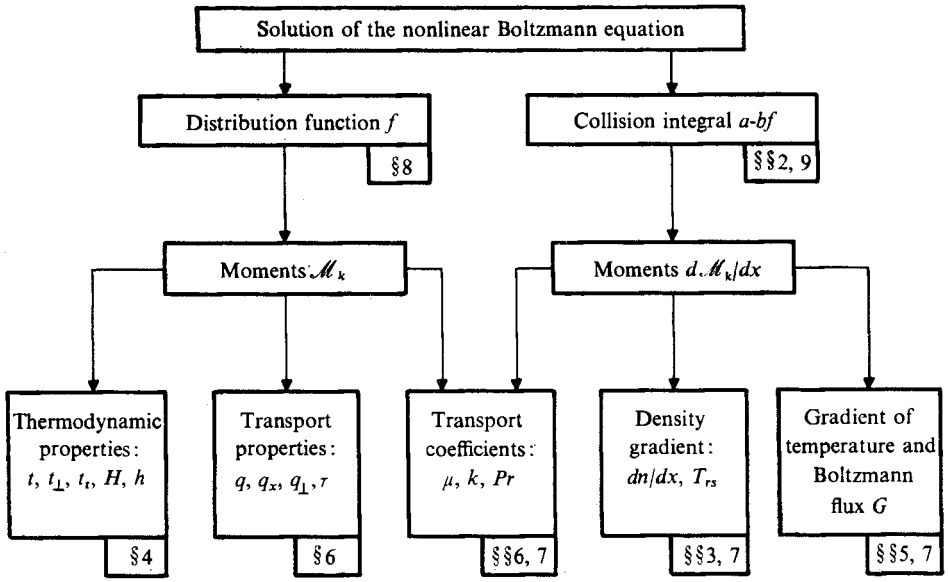

FIGURE 1. Overall method of computation of shock wave properties from the solution of the Boltzmann equation. x is the co-ordinate perpendicular to the plane of the shock, $\mathscr{M}_k$ is the kth moment of f, $d\mathscr{M}_k/dx$ the kth moment of df/dx, T_{rs} the reciprocal shock thickness, H the Boltzmann function, $h = H/n$, $t_\perp$ the lateral temperature, t_t the total temperature, q the heat flux, τ the stress, μ the viscosity coefficient and k the thermal conductivity.

moments give surprisingly good accuracy despite the error in the distribution function itself.† Also, since many other proposed shock wave models have been compared with the Mott-Smith shock, the difference between our Monte Carlo solutions of the Boltzmann equation and these models could also be easily computed.

Bird (1965, 1967, 1970*a*) used a direct simulation technique to obtain shock wave solutions. He offered a proof (Bird 1970*b*) that his procedure can be related to the Boltzmann equation and concluded that the results obtained constitute a solution of the Boltzmann equation. He computed the density profile in shock waves of the gas of elastic spheres for Mach numbers ranging from 1·5 to 30 (Bird 1965) and obtained the results on temperatures (for Mach numbers of 1·5, 3 and 10) and velocity distribution functions (for Mach number of 10) based on the longitudinal and lateral velocity components (Bird 1967). His more accurate calculations given in his recent paper (Bird 1970*a*) include those of the density profile, the reciprocal shock thickness and several higher moments of the distribution function. In addition the velocity distribution function is illustrated for $M_1 = 8$ by computer display photographs with the molecules represented as dots in the two-dimensional velocity space. Higher order moments were given for a shock wave of $M_1 = 8$ in a gas of inverse twelfth power molecules. Comparison has been made with the Mott-Smith and the Navier–Stokes shocks. We shall make several comparisons with his 1970 calculations.

† It is therefore clear that it would *not* be possible to establish the accuracy of any proposed solution $f(\mathbf{v}, x)$ solely on the basis of a few moments of the distribution function.

2. Measures of departure from equilibrium

Shock waves are interesting phenomena in rarefied gasdynamics because their interiors exhibit large departures from thermal equilibrium. It is therefore appropriate to discuss measures of this departure before discussing other aspects of shock waves. A monatomic gas is in a state of thermal equilibrium if it has a Maxwell–Boltzmann velocity distribution function. One measure, then, of the departure of a gas from thermal equilibrium is the deviation of its velocity distribution function $f(\mathbf{v})$ (obtained by solution of the Boltzmann equation) from the Maxwell–Boltzmann form. We may write the deviation as

$$\delta f = f - f_{\mathrm{eq}}, \tag{1}$$

where f_{eq} is a Maxwell–Boltzmann function that corresponds to the same values of density n, gas velocity u and temperature (or total energy) t. Since the Krook model of the collision integral is proportional to δf this measure is essentially just the Krook collision integral. (The function f is *not*, in general, a solution of the Krook equation.)

A monatomic gas is also known to be in a state of thermal equilibrium if the Boltzmann collision integral vanishes. Thus a second measure of the departure from thermal equilibrium is the deviation of the collision integral from zero. We write this in fractional form as

$$\delta\gamma = (a - bf)/a = 1 - (bf/a), \tag{2}$$

where each of the quantities a, bf and $\delta\gamma$ is a function of $\mathbf{v}$.

In certain circumstances we are interested in the variation of δf and of $\delta\gamma$ throughout velocity space. Usually, however, we would use more global measures of departure from equilibrium, which we obtain by integrating (or summing or bounding) δf, $a - bf$, or $\delta\gamma$ over the velocity space. Some useful global measures are the following: (i) r.m.s. values of δf, (ii) r.m.s. values of $\delta\gamma$ or of related functions, (iii) maximum values of $\delta\gamma$, (iv) heat flux q and stress τ and other properties which can be calculated from moments of f, (v) moments of $a - bf$. Our calculations yield values of *each* of these measures of departure from equilibrium, but we shall discuss just three of them, the second one in this section, the fourth one in §§ 4–6, and the fifth one in §§ 3 and 5.

In our studies of the relative departure from equilibrium we have found it convenient to use a certain function of $\delta\gamma$ or of the ratio a/bf. This function is

$$\psi(a/bf) = (a - bf)/(a + bf) = \delta\gamma/(2 - \delta\gamma). \tag{3}$$

Its value runs from -1 (for $a/bf = 0$) to $+1$ (for $bf/a = 0$); for a gas in equilibrium its value is zero. The global measure of departure from equilibrium that we use is the r.m.s. value of $\psi(a/bf)$ over velocity space, which we call ψ_{ab}. The values of ψ_{ab}, for different Mach numbers and different positions in the shock waves, gives us one measure of the local departure of the gas from thermal equilibrium.

Figure 2 summarizes the degree of departure from thermal equilibrium at three positions in shock waves for Mach numbers ranging from 1·1 to 10. We notice first the very large range of values of ψ_{ab}, from $1{\cdot}3 \times 10^{-3}$ near the hot side ($\hat{n} = \frac{7}{8}$) of the weakest shock ($M_1 = 1{\cdot}1$) to 0·32 near the cold side ($\hat{n} = \frac{1}{8}$) of the

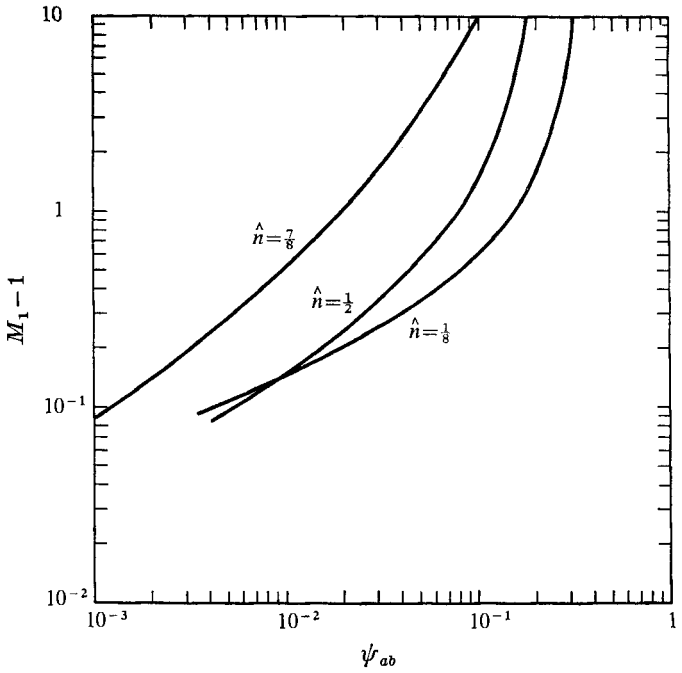

FIGURE 2. Maximum departure from thermal equilibrium in weak and strong shock waves. M_1 = Mach number, $a-bf$ = collision integral, $\hat{n} = (n-n_1)/(n_2-n_1)$, ψ_{ab} = r.m.s. value of $(a-bf)/(a+bf)$.

strongest shock ($M_1 = 10$). These two values of ψ correspond, roughly, to values of $|\delta\gamma|$ equal to 3×10^{-3} and 0·5, respectively. *Our development of Nordsieck's method of evaluation of the collision integral makes possible solutions*† *of the Boltzmann equation over this very wide range of non-equilibrium conditions.*

A second characteristic of the curves in figure 2 is noteworthy: for Mach numbers larger than about 1·2 the departure from equilibrium, as measured by ψ_{ab}, is larger near the cold side ($\hat{n} = \frac{1}{8}$) than in the centre of the shock ($\hat{n} = \frac{1}{2}$). Inspection of the isolines of ψ_{ab} show that the origin of this effect lies in the large values of $|\psi|$ (or of bf/a) for negative values of v_x, that is, corresponding to the molecules which are moving upstream relative to the shock and are being (rapidly) produced by the collisions. This non-equilibrium phenomenon, due to 'diffusion' of such high-speed molecules backwards or towards the cold side of a shock wave or other rarefied gas flow, has provoked the interest of researchers for many years.

3. Shock thickness and density gradients

As noted in § 1, we shall use n rather than x as the independent variable in giving a detailed discussion of shock structure. The present section will be concerned with the relationship between n and x. Discussion of this relation will show the nature of the $x \to n$ transformation and will also exhibit characteristics

† In the same sense as defined in § 1.

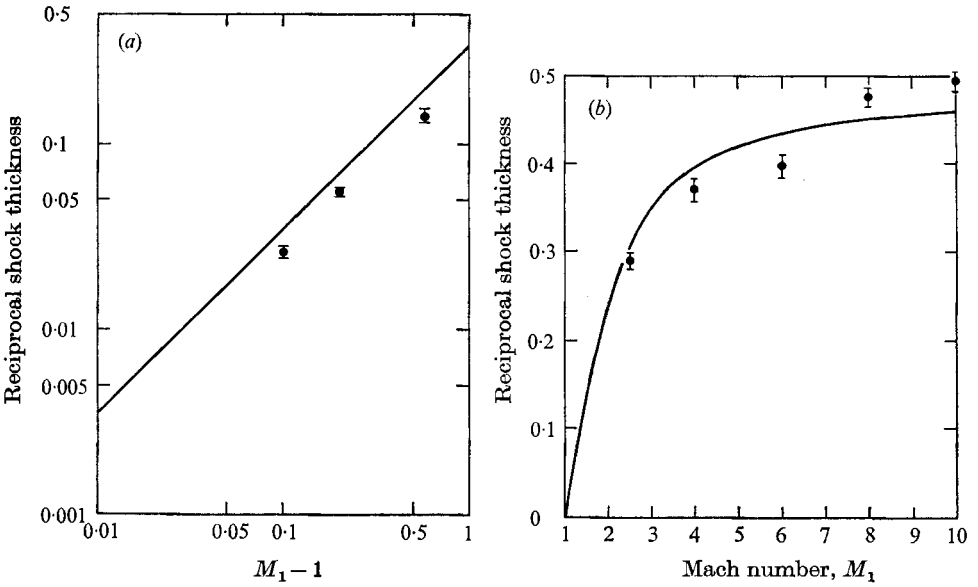

FIGURE 3. Variation of reciprocal shock thickness with Mach number M_1. ⧫, Boltzmann, showing probable error. (*a*) Weak shocks; ——, Navier–Stokes. (*b*) Strong shocks; ——, Mott-Smith (u^2 moment equation).

of the density profile in the shock waves. A comparison of Boltzmann and Navier–Stokes density gradients, for $M_1 = 1{\cdot}2$, will be given in § 7. The density profiles we obtained from the Boltzmann solutions are not symmetrical, but the asymmetry is not easy to see in an n *vs.* x plot. Also the choice of origin is arbitrary, which makes objective comparison among n–x curves from various sources rather difficult. Plotting dn/dx *vs.* $\hat{n}$ (density gradient profile) removes both these difficulties.

Just one characteristic of the density profile (or of the density gradient profile) is usually used to represent shock structure, namely, the reciprocal shock thickness T_{rs}. It is also the characteristic most commonly determined by experiment. In defining T_{rs} we first introduce the reduced density

$$\hat{n} = (n - n_1)/(n_2 - n_1), \tag{4}$$

which ranges from 0 on the cold side ($n = 1$) to 1 on the hot side ($n = n_2$). This reduced density gradient $d\hat{n}/dx$ has a maximum value $[d\hat{n}/dx]_{\max}$ somewhere within the shock, and we define†

$$T_{rs} = \sqrt{2}(d\hat{n}/dx)_{\max}. \tag{5}$$

(The unit of T_{rs} here is the upstream mean free path, not the Nordsieck unit of length.)

Our solutions of the Boltzmann equation for shock waves in a gas of elastic spheres lead to the values of T_{rs} given in figures 3 (*a*) and (*b*). We should point out that these values of T_{rs} were evaluated from the moment of the collision integral

$$n' = dn/dx = \int (a - bf)\, d\mathbf{v}/v_x,$$

† To be more specific we might call this the (density) reciprocal shock thicknesses to suggest that T_{rs} based on the profiles of other gas properties is different from T_{rs} for density.

not from the n–x curve. As shown in figure 3(a), the T_{rs} values for low Mach numbers are smaller than the corresponding Navier–Stokes results.† Since the characteristics of the Navier–Stokes shock can be described by the t–n curve and the transport coefficients together with the n–x curve, the interpretation of our comparative results for low Mach numbers will be made in § 7, in which the results for dt/dn and the transport coefficients are presented. However, we do want to point out here that the variation of properties with respect to the number density n in a Navier–Stokes shock depends on the integral curve, i.e. on the t–n relation and thus on the Prandtl number, while the determination of the variation with respect to x requires, in addition, the μ–t relation. Talbot & Sherman (1959) studied T_{rs} at low Mach numbers. They measured the temperature profile for $M_1 = 1{\cdot}335$–$1{\cdot}713$ and obtained density (or velocity) shock thicknesses (by using the *theoretical* t–n relation) that agree with Navier–Stokes shocks.

For values of $M_1 > 2{\cdot}5$, as shown in figure 3(b), we compare values of T_{rs} only with the results (using the u^2 moment) of Mott-Smith (1951). The Boltzmann and Mott-Smith values agree within the 90% confidence limits.‡ The fact that the Boltzmann T_{rs} curve and the Mott-Smith T_{rs} curve are not far apart, for intermediate values of the Mach number, does *not* imply that other shock characteristics calculated from the Boltzmann and Mott-Smith shocks are also in approximate agreement. We shall, in fact, make many other comparisons of the two shocks later in this paper.

The reciprocal shock thickness, of course, shows only one characteristic of the density profile.§ It tells us nothing about the physically interesting relaxation rates in the wings of the shock nor about the asymmetry of the density gradient profiles. The degree of asymmetry of the profiles is exhibited directly in plots of our calculated values of dn/dx *vs.* $\hat{n}$, see figure 4. The density profiles, if needed, can be calculated by numerical integration:

$$x(\hat{n}) = \int_{\hat{n}=\frac{1}{2}}^{\hat{n}} (dx/d\hat{n})\, d\hat{n}.$$

We remark first that the four curves for *each individual Monte Carle sample are smooth and of similar shape* (i.e. the four curves are 'nested'). It is therefore permissible to make a somewhat more detailed analysis of the shape of the (average) density gradient curves than would be justified by the values of ϵ_{50} shown in figure 4.

Comparison of ordinates for symmetrically placed values of $\hat{n}$ affords one test of asymmetry. On this basis we see that the gradient curves are asymmetric for all Mach numbers except those near $M_1 = 2{\cdot}5$. The asymmetry produces

† The T_{rs} curve for Navier–Stokes for $M_1 = 1$–2 is obtained from calculations of the algebraic theory (Hicks & Yen 1967). This curve deviates, on the average, by 1·6% from Wang-Chang's (1948) result for $M_1 = 1$–$1{\cdot}2$, by 3·8% from Grad's (1952) result for $M_1 = 1{\cdot}2$, and by less than 1% from Schmidt's (1965) numerical results for $M_1 = 1{\cdot}2$–2.

‡ The 90% confidence limit $\epsilon_{90} = 3{\cdot}07\epsilon_{50}$, where ϵ_{50} = probable errors which are given in most figures.

§ Grad (1952) suggested a definition of the shock thickness based on the integral properties of the profile.

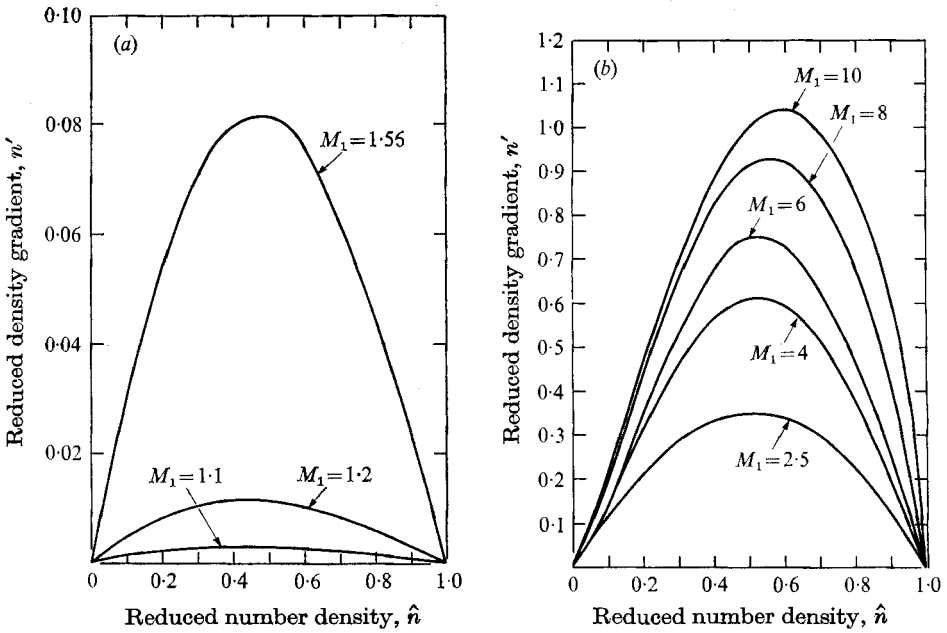

FIGURE 4. Variation of density gradient with reduced density $\hat{n}$ for various values of M_1.

M_1	1·1	1·2	1·56	2·5	4	6	8	10
Average probable error	0·00010	0·00023	0·00114	0·00892	0·0222	0·0386	0·0168	0·0194

larger upstream than downstream gradients for $M_1 < 2{\cdot}5$ and smaller upstream than downstream gradients for $M_1 > 2{\cdot}5$. These qualitative results for high Mach numbers were anticipated in our algebraic theory (Hicks & Yen 1967).

We can connect the asymmetry *within* the shock to the density relaxation rates in the shock wings by generalizing part of the Mott-Smith *Ansatz*. Thus we assume that as $x \to -\infty$

$$dx/d\hat{n} \sim a_1/\hat{n}, \tag{6}$$

and as $x \to +\infty$

$$dx/d\hat{n} \sim a_2/(1-\hat{n}). \tag{7}$$

The same relation, with $a_1 = a_2$, follows directly from the linear dependence of f on $\hat{n}$ in Mott-Smith's *Ansatz*. A simple form for the $\hat{n}$ dependence of $dx/d\hat{n}$ that satisfies both these conditions is

$$\frac{dx}{d\hat{n}} = \frac{a_1}{\hat{n}} + \frac{a_2}{1-\hat{n}} = \frac{a_1 + (a_2 - a_1)\,\hat{n}}{\hat{n}(1-\hat{n})}. \tag{8}$$

The linear expression $a_1 + (a_2 - a_1)\,\hat{n}$ is thus a correction factor for the symmetric function $\hat{n}(1-\hat{n})$. For $a_2 > a_1$ (slower relaxation per unit path downstream than upstream) the gradient curves are skewed to the left, while for $a_2 < a_1$ (faster relaxation downstream than upstream) the gradient curves are skewed to the right. By applying these results to figures 4(*a*) and (*b*), we see qualitatively that for $M_1 < 2{\cdot}5$ the upstream relaxation rate must be greater than the downstream rate, and that the reverse is true for $M_1 > 2{\cdot}5$.

M_1	$\hat{B}_1$	$\hat{B}_2$	Δ_B
1·1	0·088	0·053	0·044
1·2	0·176	0·105	0·088
1·56	0·40	0·29	0·24
2·5	0·62	0·69	0·49
4·0	0·70	1·00	0·76
6·0	0·74	1·37	0·96
8·0	0·74	1·85	1·08
10·0	0·74	2·3	1·18

TABLE 1. Parameters of the density profile in Boltzmann shock waves (elastic spheres).

The new *Ansatz* describes our data qualitatively but not quantitatively. To represent the Monte Carlo results within the tolerance given by the 90 % limits we modify it again, assuming now that

$$\hat{B} = [\hat{n}(1-\hat{n})]^{-1}(d\hat{n}/dx) = \left[\frac{1}{a_1+(a_2-a_1)\hat{n}} + \Delta_B \hat{n}(1-\hat{n})\right]. \tag{9}$$

The quantity $\hat{B}$ reduces to the asymptotic relaxation rates $B_1 = a_1^{-1}$ and $\hat{B}_2 = a_2^{-1}$ in the wings.

Equation (9) was fitted to the data of figure 4. In the wings ($\hat{n} \leqslant \frac{1}{16}$ or $\hat{n} \geqslant \frac{15}{16}$) the values of $[\hat{B} - \Delta_B \hat{n}(1-\hat{n})]^{-1}$ computed from the solution of the Boltzmann equation show large deviations above and below the values $a_1 + (a_2 - a_1)\hat{n}$. In the intermediate range ($\frac{1}{16} < \hat{n} < \frac{15}{16}$) the two sides of the equation agree to within less than the 90 % confidence limits of the left-hand side.

The resulting values of $\hat{B}_1$, $\hat{B}_2$ and Δ_B are shown in table 1. The three coefficients are each proportional to $(M_1 - 1)$ for $M_1 \leqslant 1{\cdot}56$. The relaxation rate $\hat{B}_2$ is proportional to M_1 for $M_1 >$ about 7. The relaxation rate $\hat{B}_1$ seem to approach an asymptotic value of about 0·7 as $M_1 \to 10$. The two rates appear to be equal for $M_1 \sim 2{\cdot}1$, in agreement with our earlier qualitative conclusion.

We emphasize that the values of $\hat{B}_1$, $\hat{B}_2$ and Δ_B in table 1 are tentative. When used in (9) they describe our present Monte Carlo results. However, the strong evidence for asymmetry and the estimates made of the magnitude of the relaxation rates in the wings will, we hope, stimulate further experimental and theoretical studies of the density gradient profiles of shock waves.

Shock wave theories for low Mach numbers describe $\hat{B}$ by various functions of $\hat{n}$. For example, $\hat{B}$ for Grad's thirteen-moment shock is a linear function of $\hat{n}$ with positive coefficients. The fact that the asymmetry for this shock is to the right is obvious; however, the relaxation rate in the wings cannot be explicitly determined. As the Mach number approaches one, the density profile becomes symmetric for all shock wave theories for low Mach numbers; therefore, each first-order theory for very low Mach numbers gives a constant value of $\hat{B}$.

Schmidt (1969) introduced a measure of the asymmetry of the density profile which in our notation and independent variable $\hat{n}$ has the following expression:

$$Q = \int_0^{\hat{n}_{\max}} \frac{\hat{n}}{d\hat{n}/dx} d\hat{n} \Big/ \int_{\hat{n}_{\max}}^1 \frac{1-\hat{n}}{d\hat{n}/dx} d\hat{n}, \tag{10}$$

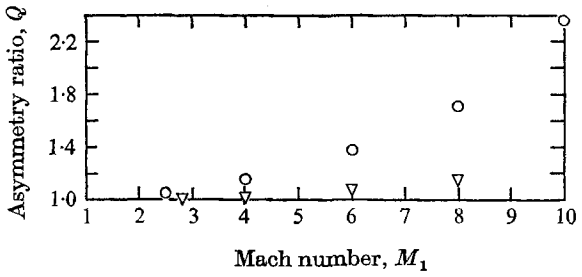

FIGURE 5. Variation of asymmetry ratio Q with Mach number M_1.

$$Q = \left\{\int_0^{\hat{n}_{\max}} [\hat{n}/(d\hat{n}/dx)]\,d\hat{n}\right\} \Big/ \left\{\int_{\hat{n}_{\max}}^1 [(1-\hat{n})/(d\hat{n}/dx)]\,d\hat{n}\right\}.$$

○, Boltzmann (elastic spheres); ▽, experiment by Schmidt (argon).

where $\hat{n}_{\max}$ = the reduced number density for maximum density gradient. Combining (9) and (10) and using the values of $\hat{B}$ given in table 1, we have computed the ratio Q for $M_1 = 2{\cdot}5$, 4, 6, 8 and 10 and compared the values obtained with the results obtained from Schmidt's experiment for argon in this range of Mach number. As shown in figure 5, our values of Q are much larger than those of Schmidt and the difference increases as M_1 increases. We should also like to point out that our solutions would yield values of Q smaller than 1 for Mach numbers lower than about 2·2, indicating that the peak of the density profile moves to the cold side of the shock wave.

4. Shock properties as functions of Mach number

In §§ 4–6 we shall discuss a number of functions derived from our solution of the Boltzmann equation for shock waves. In preparation for this discussion we shall now define a number of properties which are derived from the velocity distribution function $f(\mathbf{v}, x)$. We shall then describe the behaviour, as functions of M_1, of certain of these properties, especially those which possess extrema within the shock waves.

From six moments of the velocity distribution function f we can calculate all the ordinary macroscopic properties of the non-equilibrium gas. The six moments are $n = \mathscr{M}_1$, and $\mathscr{M}_2$, $\mathscr{M}_3$, $\mathscr{M}_4$, $\mathscr{M}_6$ and $\mathscr{M}_9$, where

$$\mathscr{M}_k = \int f \Phi_k \, d\mathbf{v}, \tag{11}$$

and

$$\Phi_1 = 1, \quad \Phi_3 = v_x^2, \quad \Phi_6 = v_x^3,$$
$$\Phi_2 = v_x, \quad \Phi_4 = v_x v^2, \quad \Phi_9 = v_\perp^2.$$

The moments $\mathscr{M}_2$, $\mathscr{M}_3$ and $\mathscr{M}_4$ are the invariants.

Our calculations show that each of five moments of f ($\mathscr{M}_6$, $\mathscr{M}_9$ and three higher moments) is nearly a linear function of n, that is, f and its moments are rather similar to the Mott-Smith f and its moments, which are *exactly* linear functions of n. The maximum deviations from linearity amount to $-0{\cdot}59$ and $1{\cdot}8\,\%$ for the moments $\mathscr{M}_6$ and $\mathscr{M}_9$, for example, for $M_1 = 2{\cdot}5$ (Hicks & Smith 1967). The

Monte Carlo fluctuations are much smaller than these deviations. Rather than showing, in this section, the detailed variation of the moments $\mathscr{M}_6$ and $\mathscr{M}_9$ with n, we shall instead discuss the characteristics of the derivatives of various related quantities in §§ 5 and 6.

The reduced dimensionless properties derived from some of the six moments are as follows.

Gas velocity	$u = \mathscr{M}_2/n.$	(12)
Lateral temperature	$t_\perp = \pi\mathscr{M}_9/n.$	(13)
Stress	$\tau = \frac{2}{3}n(t_\perp - t_x).$	(14)
Total heat flux	$q = (2\pi\mathscr{M}_4/\mathscr{M}_2) - 3t_x - 2t_\perp - 2\pi u^2.$	(15)
Longitudinal heat flux	$q_x = (2\pi\mathscr{M}_6/\mathscr{M}_2) - 3t_x - 2\pi u^2.$	(16)

In accordance with our definition of units, the units of the dimensional quantities (corresponding to the dimensionless quantities u, t, τ and q) are, respectively, u_1, t_1, p_1 and u_1^2.

To calculate the gas temperature t we need t_x, the longitudinal temperature, but this is a function of n which can be derived explicitly from the first two conservation equations (Yen 1966):

$$t_x = 2\pi[-u^2 + (\mathscr{M}_3/n)]. \tag{17}$$

The temperature and pressure of the 'reference gas' are then given by

$$t = \tfrac{1}{3}t_x + \tfrac{2}{3}t_\perp, \tag{18}$$

$$p = nt. \tag{19}$$

Knowing n and t we can calculate any thermodynamic property of the equilibrium reference gas, such as the entropy S per unit volume, for example:

$$S = n[\log(nt^{-\frac{3}{2}}) - \tfrac{3}{2}]. \tag{20}$$

The foregoing discussion shows that $t_\perp$ occupies a special place in shock theory. Unlike t_x, its dependence on n *cannot* be derived from conservation equations but must be calculated from a solution f of the Boltzmann equation for the shock and subsequent calculation of $\mathscr{M}_9/n$ by numerical integration. However, once $t_\perp(n)$ is known, the temperature t and the properties τ and q can be computed as functions of n from (11)–(18). The variation of $t_\perp$ with $\hat{n}$ is represented (indirectly) in § 5 by the variation of $d\hat{t}/d\hat{n}$ with $\hat{n}$.

There are two other important macroscopic properties of the non-equilibrium gas: the two Boltzmann functions

$$H = \int f \log f \, d\mathbf{v}, \tag{21}$$

and

$$G = \int v_x f \log f \, d\mathbf{v}. \tag{22}$$

These are seldom discussed because their calculation requires knowledge of the velocity distribution function (which can only be calculated accurately by our method for gases that are far from equilibrium) and because the integrations must then be performed by quadrature.

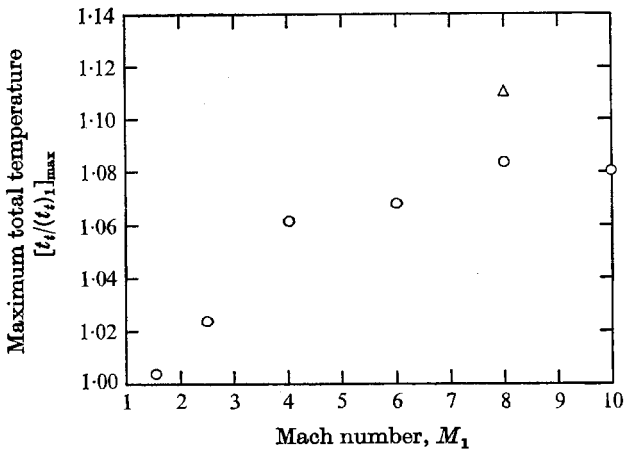

FIGURE 6. Variation of maximum total temperature $[t_t/(t_t)_1]_{max}$, with Mach number M_1. (See figure 9 for locations of these maxima.) ○, Boltzmann (maximum probable error < 0·75 %); △, Bird ($\nu = 12$).

The Boltzmann theorem for a steady-state flow, as in a shock wave, says that G must decrease monotonically through the shock. We shall make a sensitive test of the conformity of our results to this theorem in § 5. We shall see shortly that H (and the related function $h = H/n$) also possess certain other interesting properties in shock waves.

With these preliminaries out of the way we shall now discuss four properties, each a functional of f and each exhibiting a maximum within the shock waves.

It was noticed many years ago (by Nordsieck in 1959, by Hicks in 1963, see Yen (1966)) that the longitudinal temperature t_x, as a function of n in the shock (equation (17)), possesses a maximum for $M_1^2 \geqslant 1{\cdot}8$. According to the results of our Boltzmann calculations the lateral temperature $t_\perp$ does not show a maximum for any Mach number or position in the shock. The existence of a maximum of t_x thus ensures that for $M_1^2 > 1{\cdot}8$ the temperatures are not in equlibrium.

The total temperature

$$t_t = t + \tfrac{2}{5}\pi(\mathscr{M}_2/n)^2. \tag{23}$$

Its variation thus depends on two moments, $\mathscr{M}_1$ and $\mathscr{M}_2$. We have found that it has a maximum for all the Mach numbers studied. As is shown in figure 6, this maximum is less than 1·085, and the maximum t_t obtained by Bird (1970*a*) for $M_1 = 8$ and a gas obeying the twelfth-power law (force $\sim r^{-\nu}$, where $\nu = 12$, r = distance of colliding molecules) is larger than our calculation for elastic spheres at this Mach number.

For weak shocks, the Boltzmann function per unit volume (H) and the entropy per unit volume (S) are nearly equal. For strong shocks, the difference between the two functions is thus a global measure of departure from thermal equilibrium (see also § 2). At the upstream and downstream boundaries the two functions are exactly equal, so that the difference must possess an extremum inside the shock. The difference $(\hat{H} - \hat{S})$ is plotted in figure 7 for the mid-shock position to show its general behaviour as a function of M_1.

It was also noticed some time ago (Morduchow & Libby 1962) that the value

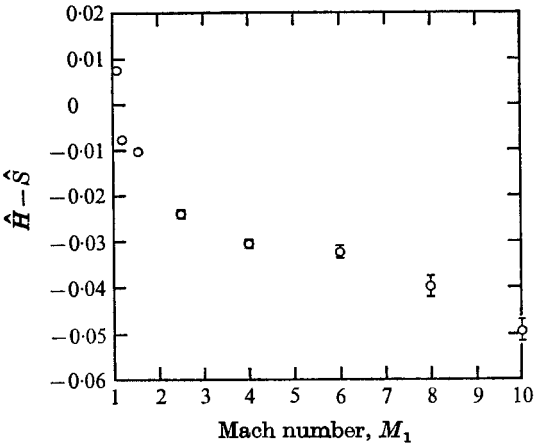

FIGURE 7. Variation of difference between the reduced Boltzmann function $\hat{H}$ and the reduced entropy $\hat{S}$ at mid-shock position ($\hat{n} = \frac{1}{2}$) with Mach number M_1. ⊙, Boltzmann, indicating probable error.

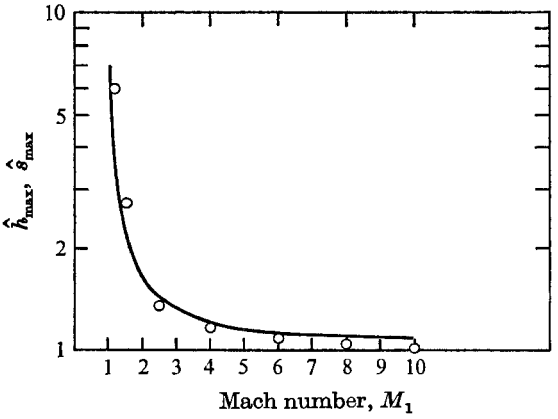

FIGURE 8. Comparison of maximum of reduced Boltzmann function per molecule, $\hat{h}_{max}$, with the Navier–Stokes value of maximum entropy per unit mass, $\hat{s}_{max}$, as a function of Mach number M_1. ——, $\hat{s}_{max}$ for Navier–Stokes shock; ○, $\hat{h}_{max}$ for Boltzmann shock (maximum probable error < 0·5 %).

of s, the entropy *per molecule*, calculated from the Navier–Stokes description of a shock wave possesses a maximum within the shock wave for all Mach numbers. The maximum is caused by the change of sign of the (large) heat-conduction term $d(k\,dt/dx)/dx$, which dominates the (smaller) positive viscous-dissipation term $\frac{4}{3}\mu\,du/dx$ (Morduchow & Libby 1962). It is therefore of interest to examine the behaviour of the maximum of the corresponding Boltzmann function $h_{max} = (H/n)_{max}$ as a function of the Mach number M_1. We find that it has the same qualitative behaviour as $s_{max} = (S/n)_{max}$ of the Navier–Stokes shock, as shown in figure 8.

We have now discussed many of the functions that possess maxima within the shock wave: n' in § 3 and t_x, t_t, $\hat{H}-\hat{S}$ and $\hat{h}$ in the present section. In figure 9 we compare the positions of the maxima of four of these functions, n', t_x, t_t, and h, for

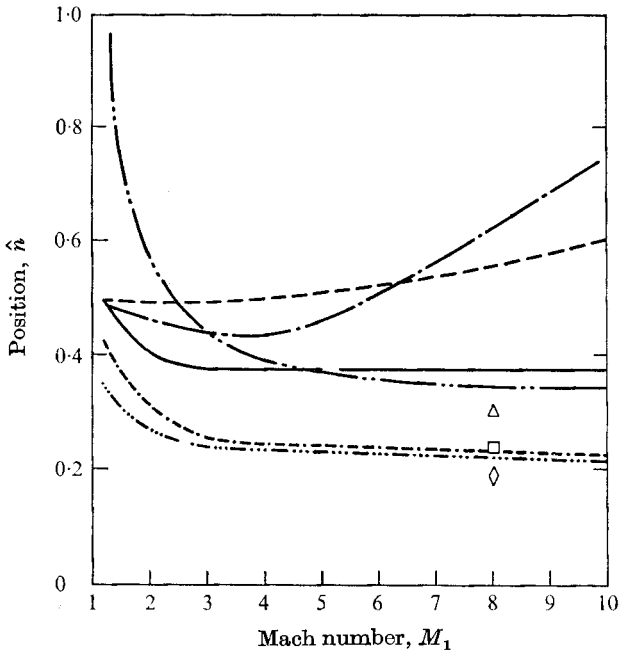

FIGURE 9. Variation of location of the maximum with Mach number M_1 for the following: longitudinal temperature t_x, Boltzmann function h, density gradient n', total temperature t_t, maximum stress τ and maximum heat flux q. —··—, t_x; —·—, h; — — —, n'; —···—, t_t; ——, τ; — —·— —, q. Results of Bird ($\nu = 12$): △, maximum stress; □, maximum heat flux; ◇, maximum total temperature.

different Mach numbers. We shall discuss the stress τ and the heat flux q in § 6 but also show in this figure the positions of the maxima of τ and q. (The positions of the maxima for τ, q, and t_t obtained by Bird (1970*a*) for $M_1 = 8$ and $\nu = 12$ are also included for comparison.)

It is clear that no one position (value of $\hat{n}$) within shock waves has a special significance for all shock properties and all Mach numbers.

5. Profiles of the gradients of shock properties

In this section we shall look at the detailed variations, for each Mach number, of several shock characteristics as functions of the independent variable n. The functions are the Boltzmann flux, defined in (22), the temperature t and the total temperature t_t. In each case we shall study the n derivatives of the function.

Since we evaluate the Boltzmann collision integrals, the gradient $\mathscr{M}'_k$ of a moment of the velocity distribution with respect to x can be evaluated from the corresponding moment of the collision integral as follows:

$$\mathscr{M}'_k = \int \Phi_k(a - bf)\, d\mathbf{v}/v_x, \tag{24}$$

where $a - bf$ = collision integral. It is convenient, in our study, to look at the gradient with respect to n:

$$d\mathscr{M}_k/dn = \mathscr{M}'_k/\mathscr{M}'_1, \tag{25}$$

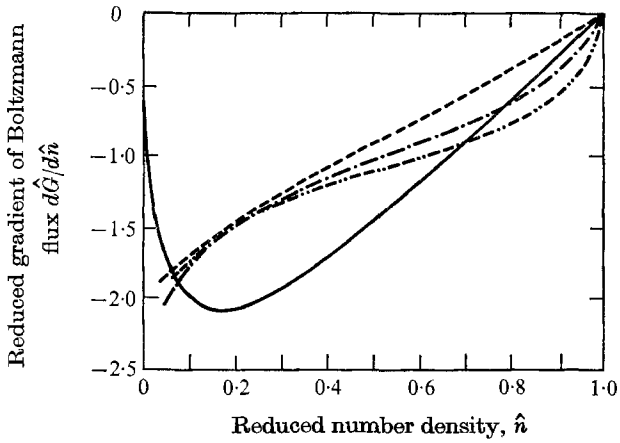

FIGURE 10. Variation of the gradient $d\hat{G}/d\hat{n}$ of the reduced Boltzmann flux with the reduced density $\hat{n}$ for various values of M_1.

	———	– – – –	—·—·—	– – ·· – –
M_1	1·56	2·50	6·00	10·00
Average probable error	0·103	0·0156	0·0753	0·0396

where $\mathscr{M}'_1 = n' =$ density gradient $= \int (a - bf)\, dv/v_x$. The gradient of any property could be obtained from those of its related moments. For example, (12), (13), (17) and (18) are used to evaluate the gradient of temperature, dt/dn, as follows:

$$dt/dn = \tfrac{2}{3}\pi\{[-\mathscr{M}_3/\mathscr{M}_1 + 2u^2 - \mathscr{M}_2/\mathscr{M}_1] + \mathscr{M}'_2/\mathscr{M}'_1\}/\mathscr{M}_1. \tag{26}$$

According to the Boltzmann theorem for steady flow of a gas

$$dG/dx \leqslant 0 \tag{27}$$

throughout the gas. Since dn/dx is positive throughout each shock wave (see § 3) the theorem can also be stated in the form

$$dG/dn \leqslant 0. \tag{28}$$

One test of the physical validity of our solutions of the Boltzmann equation is the following question: Do the solutions satisfy the Boltzmann theorem? The answer, for our solutions, is yes for the complete range of Mach number from 1·1, where the largest value of $d \log_e G/dn$ is about 10^{-5}, to a Mach number of 10, where this derivative is as large as 0·306. The rather similar Mott-Smith velocity distribution functions also satisfy the theorem. (This has not been shown analytically but is a result of our numerical calculations.) Agreement with the Boltzmann theorem is clearly one criterion that any supposed solution of the Boltzmann equation should satisfy.

The detailed variation of dG/dn with n is conveniently represented in terms of the reduced quantity $d\hat{G}/d\hat{n}$, which is plotted *vs.* $\hat{n}$ for four Mach numbers in figure 10. Notice that $d\hat{G}/d\hat{n}$ is almost independent of M_1 at the mid-shock position for M_1 greater than about two.

The derivative dt/dn is a function worth studying for several reasons. First, the Navier–Stokes treatment of the shock wave is based on this function. In particular, the value of this derivative fixes the quantitative nature of the

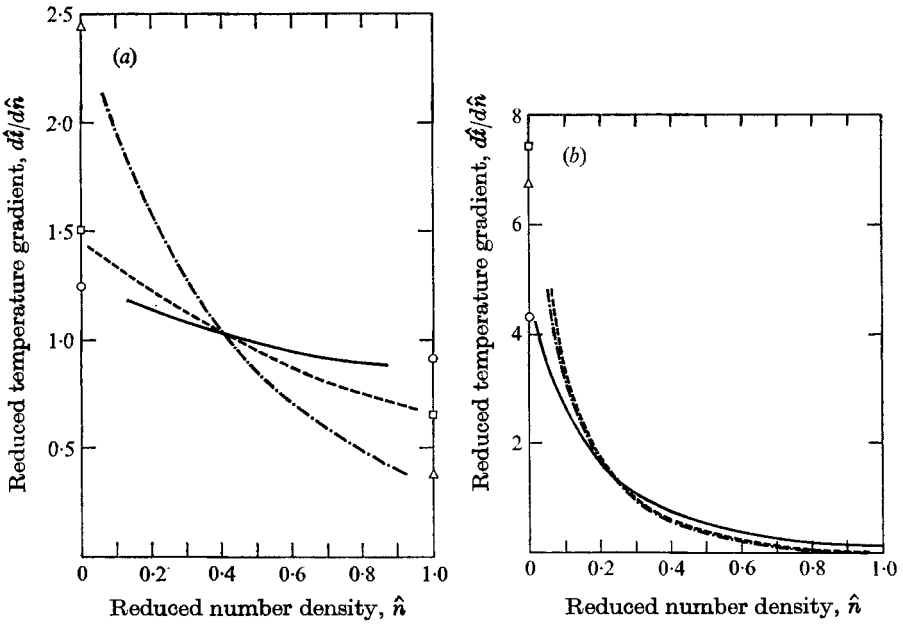

FIGURE 11. Variation of the gradient $d\hat{t}/d\hat{n}$ of reduced temperature with the reduced density $\hat{n}$ for various values of M_1.

		Boltzmann			Navier–Stokes asymptotic values		
		——	– – –	—·—·—	○	□	△
(a)	M_1	1·1	1·2	1·56	1·1	1·2	1·56
	Average probable error	0·00259	0·00642	0·00396	—	—	—
(b)	M_1	2·5	6·0	10·0	2·5	10·0	6·0
	Average probable error	0·0183	0·0227	0·0187	—	—	—

singularities at each boundary of the Navier–Stokes shock. Second, this function enters explicitly into the formula for the (effective) Prandtl number which we shall discuss in § 7. We shall therefore compare the values of dt/dn obtained from the Navier–Stokes and from our own solutions of the Boltzmann equation.

The values of $d\hat{t}/d\hat{n}$, the reduced derivative, are plotted *vs.* $\hat{n}$ for six Mach numbers in figure 11. The Navier–Stokes values of the derivative are marked on the plots at $\hat{n} = 0$ and 1 and agree well with the Boltzmann values for low Mach numbers.

The derivative dt/dn is related to the number density and the derivative of the total temperature t_t by the equation

$$dt/dn = \tfrac{4}{5}\pi(\mathscr{M}_2^2/n^3) + dt_t/dn. \tag{29}$$

Since, as has been discussed by Bagnoff & Nathenson (1970), for example, the change in total temperature is rather small in a shock wave, we would then expect dt/dn to be a rather steep function of n, varying somewhat like the inverse cube of n, as is illustrated in figure 11 (*a*). The values of $d\hat{t}_t/d\hat{n}$ are much smaller than $d\hat{t}/d\hat{n}$, but these small values represent the part of the variation of $d\hat{t}/d\hat{n}$ with $\hat{n}$ which is *not* predictable *a priori* from the term $4\pi\mathscr{M}_2^2/5n^3$ and which can only be calculated at present from solutions of the nonlinear Boltzmann equation.

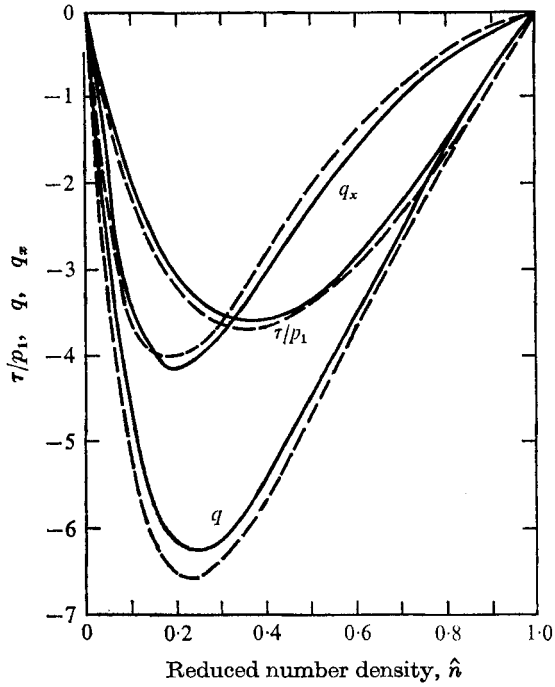

FIGURE 12. Variation of stress τ/p_1, heat flux q, and heat flux associated with longitudinal motion q_x with reduced density $\hat{n}$ for $M_1 = 4$. — —, Mott-Smith; ——, Boltzmann. Average probable error = 0·0612, 0·109 and 0·0559 for τ/p_1, q and q_x respectively.

Note also, for strong shocks, that near the hot side dt/dn is much less than either $|dt_x/dn|$ or $dt_\perp/dn$, i.e. there is a delicate balance between the large positive value of $dt_\perp/dn$ and the large negative value of dt_x/dn.

6. Transport properties of shock waves

Three transport properties are basic to our discussion. These properties are τ, a measure of the total stress (or momentum flux), q, a reduced heat flux and q_x, the part of the heat flux associated with the longitudinal random motion of the molecules. These properties are calculated from the formulae given in § 4. As seen from (11)–(18) τ and q as functions of number density can be derived from one non-invariant moment of f, namely $\mathscr{M}_9$ (see § 4), or from the lateral temperature $t_\perp$, together with t_x and u, which are known functions of the invariant moments and therefore of M_1 and of n. To calculate q_x an additional moment must be known, namely $\mathscr{M}_6$.

We shall look at the variation of the transport properties *within* a shock wave for $M_1 = 4$. (The position of maximum τ and maximum q were shown in figure 9.) Figure 12 shows the variation of the three fluxes τ, q and q_x for the Boltzmann and the Mott-Smith shocks. At the upstream and downstream boundaries of the shock the Monte Carlo values of the three fluxes are consistent with the zero values expected there. As shown in the figure, the three profiles of the Boltzmann shock are similar to those of the Mott-Smith shock; however, the differences

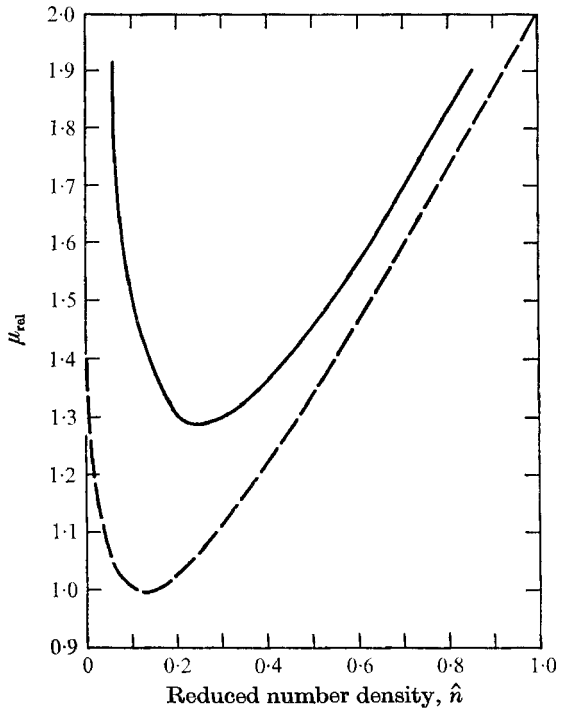

FIGURE 13. Variation of viscosity–temperature ratio $\mu_{rel} = (\mu/\mu_1)/(t/t_1)^{\frac{1}{2}}$ with $\hat{n}$ for a shock wave of $M_1 = 4$. — —, Mott-Smith; ——, Boltzmann (average probable error = 0·0797).

are significant, especially near the upstream boundary. The maximum percentage differences are 9·8 % (at $\hat{n} = 0{\cdot}125$), 21 % (at $\hat{n} = 0{\cdot}25$) and 6·5 % (at $\hat{n} = 0{\cdot}1875$) for τ, q, and q_x respectively.

In fluid dynamics one is interested in the relation between each flux and the corresponding gradient. In Navier–Stokes fluids the relation is described by the transport coefficients μ and k, defined by

$$\mu = \tfrac{4}{3}[\tau/(du/dx)], \quad k = q/(dt/dx). \tag{30}$$

For a gas of elastic spheres the temperature dependence of the coefficients is given by

$$\mu = \mu_1(t/t_1)^{\frac{1}{2}}, \quad k = k_1(t/t_1)^{\frac{1}{2}}. \tag{31}$$

In the kinetic theory of a non-equilibrium gas, like that in the interior of a shock wave, it is convenient to use the same definition of transport coefficients but to normalize them by dividing by $t^{\frac{1}{2}}$ (since we are considering elastic sphere molecules) and by the upstream value of the coefficient. Thus in our discussion we shall use

$$\mu_{rel} = (\mu/\mu_1)/(t/t_1)^{\frac{1}{2}}, \quad k_{rel} = (k/k_1)/(t/t_1)^{\frac{1}{2}}. \tag{32}$$

For a Chapman–Enskog gas (i.e. for *small* values of $M_1 - 1$) μ_{rel} and k_{rel} should be equal to one.

Figure 13 shows the variation of μ_{rel} in a shock wave for $M_1 = 4$. The values of μ_{rel} are larger near the boundaries than in the interior of the shock wave and therefore depart quite significantly from the values expected for near-equilibrium flow. (This departure is much larger for k_{rel} near the downstream boundary.)

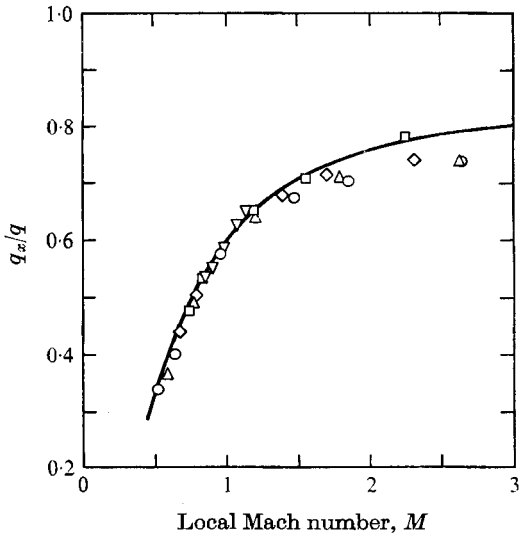

FIGURE 14. Variation of heat flux ratio q_x/q with local Mach number M for different values of M_1. ——, theory of Baganoff & Nathenson. Boltzmann: ▽, $M_1 = 1{\cdot}2$; □, $M_1 = 2{\cdot}5$; ◇, $M_1 = 4{\cdot}0$; △, $M_1 = 6{\cdot}0$; ○, $M_1 = 10{\cdot}0$.

The ratio q_x/q is also of interest. As pointed out by Baganoff & Nathenson (1970) the Chapman–Enskog approximation yields a constant value of $q_x/q = 0{\cdot}6$. Baganoff & Nathenson's (1970) model gives $q_x/q = 15M^2/(7+18M)^2$, where M = local Mach number. Our solutions of the Boltzmann equation give the results shown in figure 14, which are in good agreement with Baganoff's model. Note that even for low Mach numbers the ratio q_x/q is not a constant as predicted by Chapman–Enskog approximation, but is a function of the local Mach number. We have found that the Mott-Smith values of q_x/q do not correlate too well with the local Mach number and are much lower than Baganoff & Nathenson's curve for strong shocks.

7. Comparison with Navier–Stokes shock at a low Mach number ($M_1 = 1{\cdot}2$)

In § 3 we found that the Boltzmann results for T_{rs} are smaller than the Navier–Stokes values for low Mach numbers. In order to make a more complete comparison with the Navier–Stokes shock we shall look at four additional properties in detail for $M_1 = 1{\cdot}2$: the density gradient dn/dx, the profile of temperature t *vs.* density n, the Prandtl number Pr as a function of n, and the viscosity coefficient μ as a function of n. (We define $Pr = \frac{4}{3}(c_p\mu/k)$.)

The relevance to the weak shocks of the four properties mentioned above may be seen by reviewing here how the Navier–Stokes shock solution is usually obtained. The first step is to obtain the integral curve for constant Pr, yielding either the t–n or the t–v profile. As indicated in § 4, several properties including temperature are functions of

$$\mathscr{M}_9 = \int v_1^2 f \, d\mathbf{v};$$

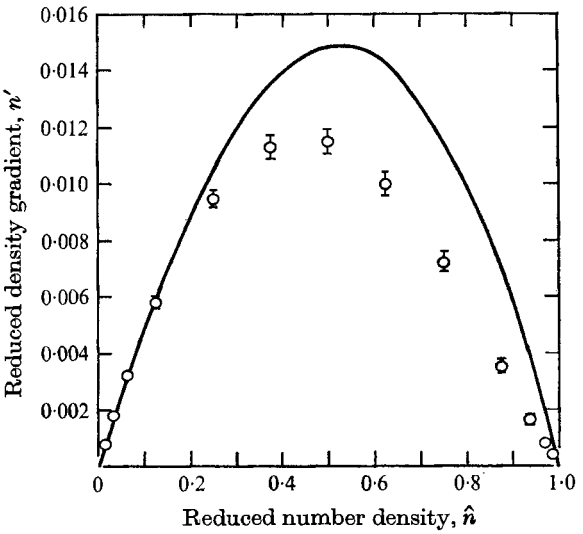

FIGURE 15. Comparison of density gradients n' of Boltzmann with Navier–Stokes results for $M_1 = 1{\cdot}2$. ——, Navier–Stokes; ϕ, Boltzmann, indicating probable error.

therefore the t–n relation also determines many other shock properties as functions of the density n. The second step is to obtain the density profile, the density n *vs.* the distance x, by using a viscosity–temperature (μ–t) relation consistent with the collision law of a gas. We see, therefore, that a Navier–Stokes shock is completely determined by four functions: $t(n)$, $Pr(n)$, $\mu(n)$ and $n(x)$.

In our study of the Boltzmann and Navier–Stokes shock for $M_1 = 1{\cdot}2$ we need (i) to look at the difference in dn/dx for the two shocks, (ii) to compare the dt/dn profiles, (iii) to examine the variation of Pr in the Boltzmann shock and (iv) to see if the viscosity coefficient in the Boltzmann shock is proportional to the square root of temperature, a relation derived from the linearized theory for elastic-sphere gases.

Figure 15 shows the variation of reduced density gradient dn/dx *vs.* reduced density $\hat{n}$. For $\hat{n} > 0{\cdot}2$, the Boltzmann values of dn/dx are significantly lower than the Navier–Stokes results. The value of T_{rs} for $M_1 = 1{\cdot}2$ shown in figure 3(a) is proportional to the maximum value of dn/dx in this figure.

The results for the reduced temperature gradient $d\hat{t}/d\hat{n}$ are compared in figure 16, which shows good agreement for the two shocks. This agreement implies good agreement also for the variation of the properties such as t, $t_\perp$, τ and q (which are functions of $\mathscr{M}_3$) as functions of the density n. Figure 17 shows the variation of Pr *vs.* $\hat{n}$ in the Boltzmann shock. The significant variation of Pr, except near the cold and hot sides, is less than 10 %. Since the Navier–Stokes dt/dn was obtained on the basis of constant Pr of $\frac{8}{9}$ (equivalent to $c_p\mu/k = \frac{2}{3}$), the Prandtl numbers within the Boltzmann shocks are also in accord with that of the Navier–Stokes shock.

The ratio $\mu_{\text{rel}} = (\mu/\mu_1)/(t/t_1)^{\frac{1}{2}}$ is equal to one for a gas of elastic spheres. We have studied this ratio for one shock ($M_1 = 4$, see § 6). The variation of this ratio for an $M_1 = 1{\cdot}2$ shock is given in figure 18. We note that this ratio is

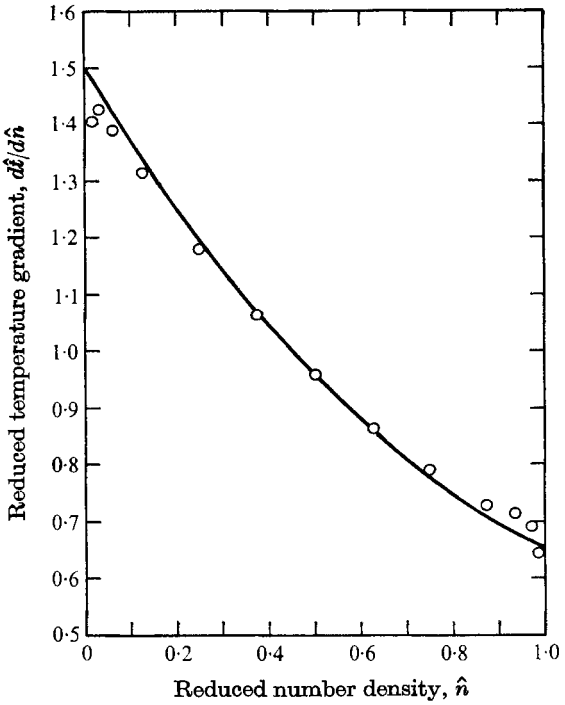

FIGURE 16. Comparison of Boltzmann gradient of reduced temperature, $d\hat{t}/d\hat{n}$, with the Navier–Stokes values for $M_1 = 1{\cdot}2$. ——, Navier–Stokes; ○, Boltzmann (average probable error = 0·00643).

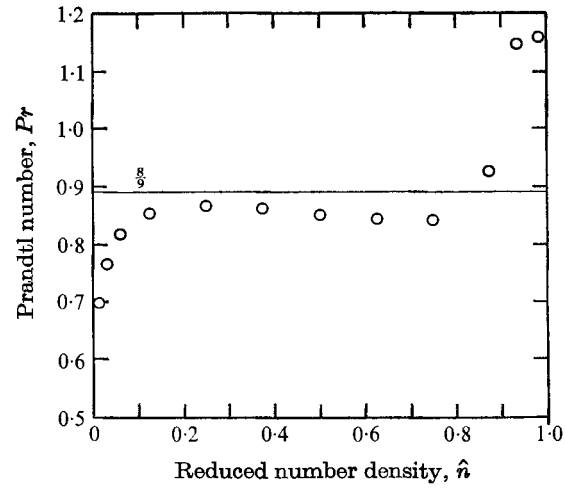

FIGURE 17. Variation of Prandtl number Pr with reduced density $\hat{n}$ for $M_1 = 1{\cdot}2$. ○, Boltzmann (average probable error = 0·0272).

definitely greater than unity on the downstream half of the shock, with a maximum departure of 40 %. The fact that the ratio μ_{rel} is greater than one for the Boltzmann shock is in accord with the fact that the Boltzmann values of dn/dx and T_{rs} are smaller than the Navier–Stokes values for $M_1 = 1{\cdot}2$ and other low Mach numbers.

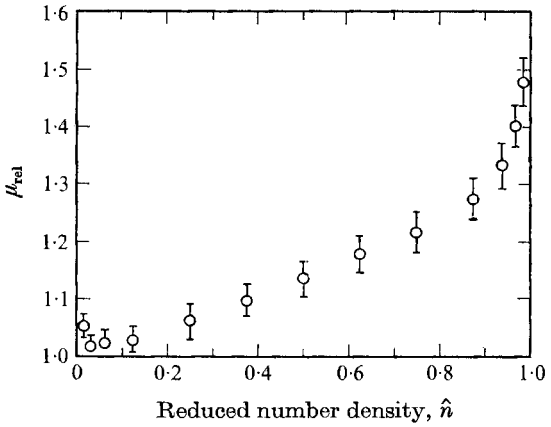

FIGURE 18. Variation of the viscosity–temperature ratio $\mu_{rel} = (\mu/\mu_1)/(t/t_1)^{\frac{1}{2}}$ with reduced density $\hat{n}$ for $M_1 = 1{\cdot}2$. $\Diamond$, probable error.

8. The velocity distribution function

In the previous sections we have discussed the dependence on Mach number and shock position of many moments of f, of the velocity distribution function, and of other functions derived from f. In this section we shall describe the behaviour of f as a function of position in velocity space for one Mach number ($M_1 = 4$) and at several positions in the shock.

The qualitative nature of the distribution function was monitored by a computer graphical display system. The layout of the velocity space for the display of our velocity-dependent functions and a representative distribution function f at the mid-shock position ($\hat{n} = \frac{1}{2}$) for $M_1 = 4$ are shown in figure 19 (plate 1). We observe the bimodal characteristics of the distribution function.

In making quantitative studies of f it is convenient to compare with the Mott-Smith values. Let us define

$$\delta f_M = f_B - f_{MS}, \tag{33}$$

each term in the equation, of course, being calculated for the same value of $\mathbf{v}$ and $\hat{n}$, and for the same Mach number (f_B and f_{MS} being Boltzmann and Mott-Smith values respectively).

The nature of the variation of δf_M across velocity space for the mid-shock position ($\hat{n} = \frac{1}{2}$) is such that there are regions in which δf_M is positive and other regions in which δf_M is negative. These regions are well defined at all positions within the shock but their shape and size vary with position. These facts suggest that the errors of the Mott-Smith function for this Mach number are indeed significant in the shock.

This opinion is confirmed when we look at values of δf_M for individual bins in comparison with the estimates we have made of $\epsilon_{90} f$ for the same bins. We find that, for about 40 % of the bins, at most shock positions δf_M is greater than $3\epsilon_{90} f$, that is, the δf_M values as large as those observed for these bins would occur by chance only once in 100 or more trials. Near the cold boundary these highly significant values of f occur only for about 20 % of the bins, so that here the Mott-Smith *Ansatz* gives fewer large deviations from the solution of the Boltz-

mann equation than elsewhere.† Nevertheless, the largest individual deviations also occur near the cold side of the shock.

The r.m.s. values of δf_M and $\epsilon_{90} f$ are each approximately constant across the shock. The r.m.s. value of δf_M for all stations ($1{\cdot}34 \times 10^{-2}$) is 1·7 times larger than the average values of $\epsilon_{90} f$ ($0{\cdot}79 \times 10^{-2}$) and is 6·3 times smaller than the r.m.s. value of f throughout the shock.

A qualitative summary of the characteristics of the Boltzmann $f(\mathbf{v}, n)$ would be useful in guiding the future development of analytical or analytical–numerical methods of describing the properties of shock waves. To do this we shall again use δf_M, the departure of f from the corresponding Mott-Smith function, because the fractional deviation $\delta f_M/f$ is generally small, though it may be large in a few local regions in velocity space and in the shock. What are the qualitative properties of δf_M obtained from our solution of the Boltzmann equation?

(i) $\delta f_M = 0$ at the upstream and downstream boundaries of the shocks.

(ii) $\delta n = \int \delta f_M d\mathbf{v}$ must be 0 because the values of f_B and f_{MS} in (33) are calculated for the same value of n. Therefore, δf_M must have both positive and negative values for each position in the shock.

(iii) The three conserved moments of δf_M, like those of f and of f_{MS}, must be constant across the shock.

(iv) δf_M cannot be represented as a product of a function of n and a function of $\mathbf{v}$ because the shape of the isolines of δf_M changes with n, i.e., with position in the shock.

(v) In particular, δf_M is not simply proportional to $\hat{n}(1-\hat{n})$, because analysis of three of the non-conserved moments of f show that it cannot be represented by quadratic functions of n.

Bird (1970*a*) has studied computer display representation of the distribution function for $M_1 = 8$ and has also found that the general behaviour gives qualitative support of the bimodal assumption of Mott-Smith but is not in agreement with the Mott-Smith solution in detail.

Muntz & Harnett (1970) have recently made two experimental measurements of certain distribution functions for $M_1 = 1{\cdot}59$:

$$F(v_x) = \int f dv_x dv_y \quad \text{and} \quad F(v_y) = \int f dv_x dv_z.$$

They found that $F(v_x)$ deviated significantly from that of the corresponding Chapman–Enskog first iterate. In order to find whether similar deviations exist between our Boltzmann results and those of Chapman–Enskog first iterate, we have made a similar comparison for $M_1 = 1{\cdot}59$ for elastic spheres. The results for the half width of $F(v_x)$ are in excellent agreement with their findings (Holtz, Muntz & Yen 1971).

We should like to point out that Muntz & Harnett's results are for helium with a different collision cross-section from that of the elastic spheres we consider. We have computed the Chapman–Enskog half width for helium (with $\mu \sim t^{0{\cdot}647}$) for $M_1 = 1{\cdot}59$ and have found no discernible difference, when the results are

† Essentially the same result was found earlier for the $M_1 = 2{\cdot}5$ shock (Hicks & Smith 1967).

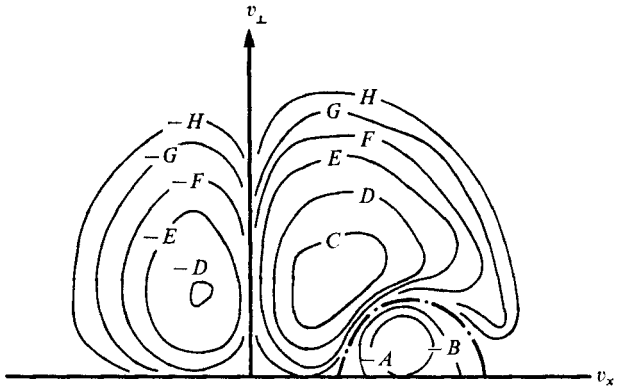

FIGURE 20. Isolines of the function $v_\perp(a-bf)$ at the mid-shock position ($\hat{n} = \frac{1}{2}$) for $M_1 = 4$. $v_\perp(a-bf)$ is the function calculated directly by Nordsieck's Monte Carlo method. Numerical values of $v_\perp(a-bf)$ in arbitrary units: A, 8000; B, 5000; C, 3500; D, 2000; E, 800; F, 350; G, 150; H, 80.

plotted *vs.* $\hat{n}$, with that of the elastic spheres. We believe, therefore, that the effect of using the actual helium cross-section on the Monte Carlo result is, for this Mach number, probably also small. However, we are planning to incorporate in our computer program other differential collision cross-sections than that of the elastic spheres and to study their effects.

Bird computed $F(v_x)$ and $F(v_\perp)$ for the shock of $M_1 = 10$ (Bird 1967).

9. The Boltzmann collision integral ($M_1 = 4$)

As pointed out in the introduction, it is Nordsieck's method of evaluation of the (nonlinear) Boltzmann collision integral that has made possible the solution of the Boltzmann equation for strong shock waves and other far-from-equilibrium situations. Since the nature of the Boltzmann collision integral, as calculated by Nordsieck's Monte Carlo method from a solution of the Boltzmann equation for the shock wave as well as the heat-transfer problems, and the comparison with the approximations to it associated with the names of Mott-Smith and Krook are discussed in detail in a separate paper (Hicks & Yen 1971), we shall describe here briefly only some of its important characteristics for $M_1 = 4$ and $\hat{n} = \frac{1}{2}$.

In figure 20 are shown the isolines of the functions $v_\perp(a-bf)$ (the function calculated directly by our numerical solution of the Boltzmann equation) at the mid-shock position ($\hat{n} = \frac{1}{2}$) for $M_1 = 4$. The negative values of the function for large positive v_x correspond to $(a-bf)/v_x = df/dx < 0$ and to the scattering loss of molecules with high forward velocity, like those characteristic of the cold side of the shock. The negative values for $v_x < 0$ (molecules moving in the upstream direction) correspond to $df/dx > 0$. The collision integral should vanish on the line $v_x = 0$ if df/dx is to be finite there. This requirement is a strong test of the reliability of numerical solutions of the Boltzmann equation or of approximations like those of Mott-Smith and Krook. Except in the case of a few velocity bins *the values of* $(a-bf)$ *obtained by Monte Carlo solution of the Boltzmann equation satisfy this criterion well.*

The authors dedicate this paper to the late Arnold Nordsieck, whose method of evaluating the Boltzmann collision integral opened a new era in the kinetic theory of gases. This work was supported in part by the Joint Services Electronics Program (Contract no. DAAB-07-67-C-0199) and the Office of Naval Research (Contract no. N00014-67-A-0305-0001).

REFERENCES

BAGANOFF, D. & NATHENSON, M. 1970 *Phys. Fluids*, **13**, 596.

BIRD, G. A. 1965 *Proc. 4th Int. Symp. on Rarefied Gas Dynamics*, **1**, 216.

BIRD, G. A. 1967 *J. Fluid Mech.* **30**, 479.

BIRD, G. A. 1970*a* *Phys. Fluids*, **13**, 1172.

BIRD, G. A. 1970*b* *Phys. Fluids*, **13**, 2676.

GRAD, H. 1952 *Comm. Pure Appl. Math.* **5**, 257.

HICKS, B. L. 1965 *C.S.L. Rep. University of Illinois*, R-236.

HICKS, B. L. & SMITH, M. A. 1967 *C.S.L. Rep. University of Illinois*, R-347.

HICKS, B. L. & SMITH, M. A. 1968 *J. Comp. Phys.* **3**, 58.

HICKS, B. L. & YEN, S. M. 1967 *Phys. Fluids*, **10**, 458.

HICKS, B. L. & YEN, S. M. 1969 *Proc. 6th Int. Symp. on Rarefied Gas Dynamics*, **1**, 313.

HICKS, B. L. & YEN, S. M. 1971 *Proc. 7th Int. Symp. on Rarefied Gas Dynamics* (to be published).

HICKS, B. L., YEN, S. M. & REILLY, B. 1969 *CSL Rep. University of Illinois*, R-412.

HOLTZ, T., MUNTZ, E. P. & YEN, S. M. 1971 *Phys. Fluids*, **14**, 545.

MORDUCHOW, M. & LIBBY, P. A. 1962 *Pibal Rep. Brooklyn Institute of Technology*, no. 749.

MOTT-SMITH, H. M. 1951 *Phys. Rev.* **82**, 885.

MUNTZ, E. P. & HARNETT, L. N. 1970 *Phys. Fluids*, **12**, 2027.

NORDSIECK, A. & HICKS, B. L. 1967 *Proc. 5th Int. Symp. on Rarefied Gas Dynamics*, **1** 675.

SCHMIDT, B. 1969 *J. Fluid Mech.* **39**, 361.

SCHMIDT, H. J. 1965 M.S. thesis, University of Illinois.

TALBOT, L. & SHERMAN, F. S. 1959 *N.A.S.A. Memo.* 12-14-58W.

WANG-CHANG, C. S. 1948 *University of Michigan Rep.* APL/JHO CM 504.

YEN, S. M. 1966 *Phys. Fluids*, **9**, 1417.

YEN, S. M. 1971 *Proc. 7th Int. Symp. on Rarefied Gas Dynamics* (to be published).

YEN, S. M. & HICKS, B. L. 1967*a* *CSL Rep. University of Illinois*, R-350.

YEN, S. M. & HICKS, B. L. 1967*b* *Proc. 5th Int. Symp. on Rarefied Gas Dynamics*, **1**, 785.

YEN, S. M. & SCHMIDT, H. J. 1969 *Proc. 6th Int. Symp. on Rarefied Gas Dynamics*, **1**, 205.

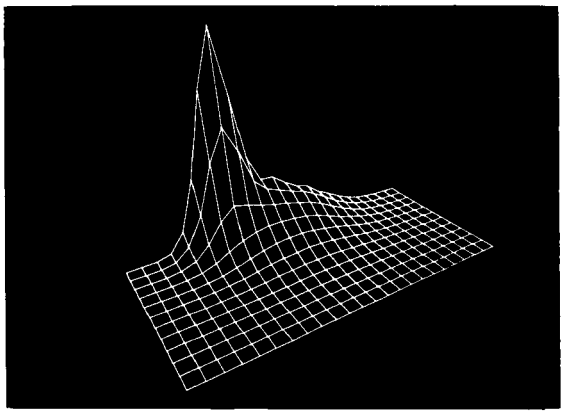

Front view

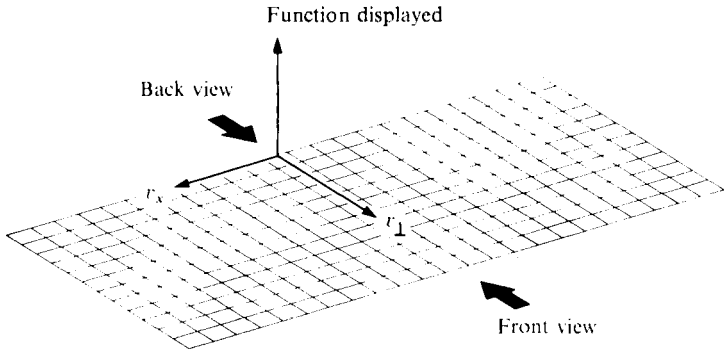

FIGURE 19. Display of distribution function f at mid-shock position ($\hat{n} = \frac{1}{2}$) for $M_1 = 4$.